Comprehensive thermodynamic analysis of steam storage in a steam cycle in a different regime of work: A zero-dimensional and three-dimensional approach

Paweł Ziółkowski[1], Natalia Szewczuk-Krypa[1], Anna Butterweck[1], Michał Stajnke[2], Stanisław Głuch[1], Marta Drosińska-Komor[1], Anna Milewska[1], Jerzy Głuch[1]

[1]Gdańsk University of Technology, Faculty of Mechanical Engineering and Ship Technology, Gdańsk, Poland

[2]Energy Conversion Department, Institute of Fluid-Flow Machinery, Polish Academy of Sciences, Gdańsk, Poland

e-mail: pawel.ziolkowski1@pg.edu.pl

Keywords: Energy conversion/systems, Energy systems analysis, Heat energy generation/storage, Power generation

Abstract

Due to the current trends aiming to reduce carbon dioxide emissions by increasing the use of renewable energy sources, changes are required in the operation of coal-fired steam units. The unstable nature of renewable energy sources, depending on weather conditions, means that the amount of energy produced varies and is not always in line with peak demand. To ensure the security and stability of energy supplies in the energy system, renewable sources should cooperate with units independent of environmental conditions. With conventional steam systems, the main issue of such energy storage applied to steam turbine units presented in the paper, which, in the event of a need for a sudden reduction of the system load, prevents overloading of the boiler and turbines, improving the safety of the system. This article presents a thermodynamic model of this energy storage. A zero-dimensional (0D) model was implemented, including the operating parameters of the unit. This model directly relates to the thermodynamic parameters defined at specific points of the thermodynamic cycle. Based on the 0D model, it was shown that the process of loading the energy storage with steam leads to a load reduction of up to 4%. On the other hand, when discharging the stored energy, the net power of the steam block may increase by 0.4%. For more detailed analysis, a three-dimensional (3D) non-equilibrium with including cross effects approach was applied. This approach is based on flow models, with phase transitions that determine temperature fields, densities, phase transition in relevant space, and is used for more accurate analysis. Here we investigate the relationship between the 0D

and 3D approaches in the context of steam storage. The combination of these two approaches is the fundamental novelty of the article.

1 Introduction

The aim of the current European Union (EU) energy strategy is to encourage activities in the low-emission area. This strategy indicates a 40% reduction in carbon emission and 30% EU-wide share for renewable energy sources (RES) by 2030 [1]. Increased exploitation of renewable energy sources makes it difficult to maintain a balance between supply and demand for electricity. Renewable energy sources mostly depend on meteorological conditions, which means that energy production is intermittent and fluctuates over time regardless of the actual consumption [2]. Energy deficits in the system resulting from the time lack of power production from renewable sources can be compensated by cooperation with a Thermal or Nuclear Power Plant. The disadvantage of this solution is the low flexibility of these systems [3]. Therefore, the application of energy storage technology could be appropriate in this cooperation. Energy storages allow for increasing energy production flexibility [4]. In addition, their great advantage is the possibility of electric grid operation safety improvement by reducing the frequency fluctuations reduction [5,6]. Energy storage in the power system also improves the economic aspect of electricity generation. The increase in renewable energy supply reduces the average market price of electricity and highly influences the price trends. It affects a significant reduction in energy price during the period of large electricity production from renewable sources and in times of low energy demand. This increases energy production prices [7].

Various types of energy storage are used in industry. These include compressed air storage facilities, pumped storage power plants, heat storage facilities, and hydrogen storage facilities [8,9]. The most popular are electrochemical methods that use electrochemical accumulators for energy storage. The pumped storage plant is also a popular solution. The disadvantage of this solution is the need to provide a large surface area for two water reservoirs: the upper one from which at the time of energy peak demand water is transferred into the lower one from which during the excess energy water is pumped to the upper reservoir [10]. Compressed air storage belongs to a mechanical method. It is very economically beneficial because air is freely available. The problem is the storage of large amounts of air under high pressure [6,11,12]. Thermal energy storage is used in gas and steam power plants and heat and

power plants equipped with gas turbines. The thermal energy can be stored by recovering it from the stream of hot exhaust gases from the gas turbine [13].

The innovative steam accumulator can be an integral part of the unit and thus responds quickly to load changes, and thus enhances the provision of primary control reserve while maintaining high efficiency of energy conversion. Concerning power plants, it improves the operational safety of generation units, as it prevents the overloading of boilers and turbines in the case of a steep reduction in the load.

Steam units are often subject to load changes when working with renewable energy sources. With a sudden increase in electricity production from, for example, wind farms, steam turbines are forced to suddenly reduce electricity production. At this point, there is a difference in the rate of change in power between the steam boiler that produces steam and the steam turbine that receives it. Excess steam can be redirected to the steam storage. In contrast, if you suddenly need to increase the power of the steam turbine, there is water in the storage facility which, when it reaches the boiler, easily turns into steam without overloading the boiler with excessive fuel. Therefore, this solution has a positive effect on the boiler, the turbine, and the whole system.

A steam power plant is able to adjust its generation swiftly to load changes and becomes more competitive on the capacity market by improving dynamic characteristics [14]. The relative disadvantage of steam storage is its limited capacity. Therefore, the articles include a comprehensive assessment of the power plant parameters that will allow developing guidelines and recommendations to determine the optimal operation modes of the steam accumulator for the case of the underlying reference process, considering changing ambient conditions and current operational requirements.

The multidimensional approach carried out here using the proposed non-stationary thermodynamic steam storage model and calibrated in experiments will allow verification of the impact of modernization proposals on: 1) power plant components, 2) basic energy indicators, 3) emission levels, 4) production efficiency, and 5) create dynamic characteristics of the steam storage.

In this study, we outline a thermodynamically justified multidimensional approach to describe the characteristics of thermal processing of steam storage in the steam cycle. The model stems from a common thermodynamic approach and from preceding papers on fluid flow in such systems dominated by various mechanisms, such as mass, momentum, and energy

transfer [15–18]. A schematic presentation of these of emerging aspects of multidimensional mathematical modeling that considers a fluid-solid interaction and volumetric integration from dynamics (3D) to mechanics (0D) is highlighted in Fig. 1.

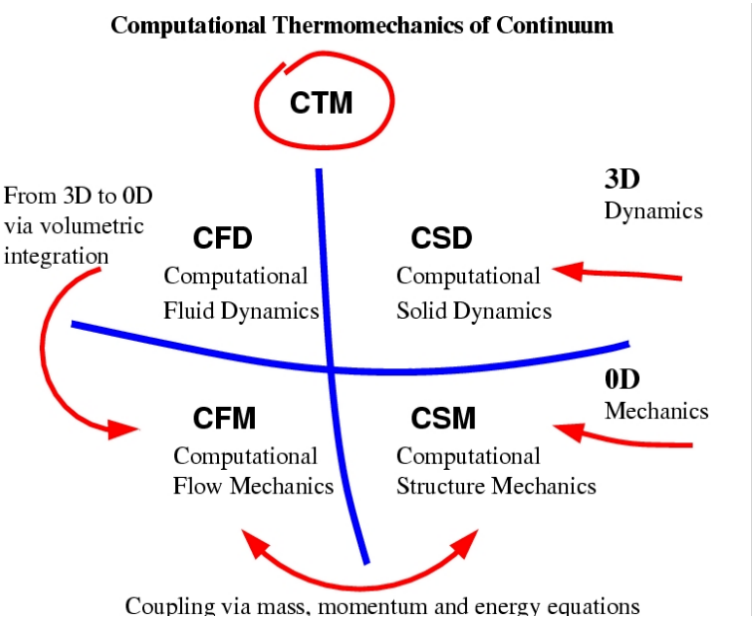

Fig. 1. Schematic presentation of emergency aspects of multidimensional mathematical modeling that takes into account a fluid-solid interaction and volumetric integration from 3D approach to 0D.

Fig. *1* shows the relationship between the numerical tools of the Computational Thermomechanics of Continuum (CTM). Computational Flow Mechanics (CFM) tools are based on integral (algebraic in space) equations of mass, momentum, and energy balance. For example, in CFM, at the engineering level (0D), treating steam storage as a "black box" which has inlets and outlets, heated surfaces on which heat is exchanged and a moving surface (phase separation surface) on which energy is absorbed or transferred to the way of work. Computational Structure Mechanics (CSM) is designed to quickly design the structure of a device based on well-known design techniques and, in the context of steam storage, will be used to design wall thicknesses and load-bearing frames and, consequently, to determine the expected stress levels and strength of the device [15–18].

1.1 From three-dimensional thermodynamic modeling to zero-dimensional equations

The transition to a higher dimension of 1D, 2D, or 3D should consider spatial changes, so the mathematical description introduces divergence. The broadest and most accurate distribution of individual thermodynamic parameters gives a three-dimensional view, which is also preferred for data transfer between solid and fluid. Traditionally, in local terms, we use two types of approaches, namely Computational Fluid Dynamics (CFD) [19] and Computational Solid Dynamics (CSD) [20,21]. CSD strength analyses derive data from CFDs and can simultaneously influence the nature of the flow as a result of displacements. On the other hand, CFD analyses affect the solid body by changing the stress state, temperature distribution, and thickness of the separation surface in case of deposition, which is shown schematically in 1. The steam accumulator itself will be analyzed in detail by means of FSI based on flow models with phase transitions induced both by change of pressure and temperature. Computational Solid Dynamics (CSD) models will be included to obtain stress, creep, and fatigue. The mathematical modeling of complex physical phenomena in steam storage meets with growing interest, particularly with regard to the energy storage of the steam cycle. Summarizing the local (3D) level used in CFD techniques, it is possible to associate the integral approach with CFM, i.e., the level (0D), by integrating the local area [22]:

$$0\mathrm{D} = \iiint_{V} (\,3\mathrm{D})\,\mathrm{d}V \tag{1}$$

where V is the volume at which integration from 3D to 0D takes place.

At this point, it is worth mentioning that the phenomenon accompanying calculations based on 3D models is a renaissance of meaning and an almost complete restoration of the equivalent significance of calculation codes based on 0D models. It should be remembered that the 0D codes covering the entire steam cycle and steam storage tank thus serve the 3D codes (both for fluid and solids) as the “giver” of boundary conditions and averaged (in the sense of 0D) load data. Furthermore, the results of 3D calculations are also compared to the results of 0D codes after averaging, especially at the design stage of the solution, when no measurement data are available yet.

1.2 Aims and scope of work

The main aim of the work is to numerically model a steam storage facility included in the steam cycle, which improves the flexibility of the operation of these systems in interaction with renewable energy sources. Section 2 presents the basic balance equations in three-dimensional and zero-dimensional terms to determine the characteristics of unit operation. Section 3 shows the thermodynamic cycle of the thermal power plant with an indication of power and efficiency in the basic system configuration and during charging and discharging. Also, the concept of steam storage location on the steam cycle scheme is described in Section 3. Section 4 shows the parameters and scheme of the tank for experimental measurements. However, the main output of this section is the 3D flow analyses which present further fields, namely density, temperature, phase transition, and volume fraction of components. The last point outlines the perspectives and conclusions from work (section 5).

The novelty of this work is to show the coupling between two levels of modeling, namely design (0D) and detailed verification (3D) for the key elements of the proposed technical solution, which is the integration of the steam storage into the thermodynamic cycle. Additionally, the mathematical model of complex physical phenomena in steam storage is of increasing interest, particularly with regard to energy storage in the steam cycle.

2 Main governing equations

In the case of steam storage, the 3D approach to flow (CFD) is complex. The area inside the storage is characterized by zones where there is liquid and gas in turn, and the individual liquids are separated by a separation area. With regard to the separation area, there are commercial VOF approaches as well as more accurate models for phase slip and surface transpiration. However, at this point, it is worthwhile to bring closer the area of strictly steam as a medium which, after entering the steam storage, undergoes significant pressure and temperature changes, causing the transition from dry steam to wet steam. For a consistent non-equilibrium condensation model, a set of nine transport equations can be written in the general form [23]:

$$\frac{\partial}{\partial t}\begin{Bmatrix}\rho\\ \rho\mathbf{v}\\ \rho e\\ \rho k\\ \rho\varepsilon\\ \rho x\\ \rho\alpha\end{Bmatrix}+\operatorname{div}\begin{Bmatrix}\rho\mathbf{v}\\ \rho\mathbf{v}\otimes\mathbf{v}\\ \rho e\mathbf{v}\\ \rho k\mathbf{v}\\ \rho\varepsilon\mathbf{v}\\ \rho x\mathbf{v}\\ \rho\alpha\mathbf{v}\end{Bmatrix}+\operatorname{div}\begin{Bmatrix}0\\ p\mathbf{I}\\ p\mathbf{v}\\ 0\\ 0\\ 0\\ 0\end{Bmatrix}=\operatorname{div}\begin{Bmatrix}0\\ \mathbf{t}^t\\ \mathbf{t}^t\mathbf{v}+\mathbf{q}^t\\ \mathbf{J}_k\\ \mathbf{J}_\varepsilon\\ \mathbf{J}_x\\ \mathbf{J}_\alpha\end{Bmatrix}+\begin{Bmatrix}0\\ \rho\mathbf{S}_\mathbf{v}\\ \rho S_e\\ \rho S_k\\ \rho S_\varepsilon\\ \rho S_x\\ \rho S_\alpha\end{Bmatrix} \qquad (2)$$

in which: ρ; $\rho\mathbf{v}$; ρe; ρk; $\rho\varepsilon$; ρx; $\rho\alpha$ represents the relevant conserved variable vector. First, three variables (ρ; $\rho\mathbf{v}$; ρe) are generated from the well-known equations: the balance of mass (ρ), the balance of momentum ($\rho\mathbf{v}$ - three scalar equations for each velocity component), the balance of energy (ρe). However, $\rho=\rho(\mathbf{x},t)$ represents the mixture density that depends on time t and location $\mathbf{x}$. Here, $\mathbf{v}=v_i\mathbf{e}_i$ is velocity vector including $\mathbf{e}_i$ (versor in direction i) and v_i (value of vector $\mathbf{v}$). $\rho\mathbf{v}$ can be named the momentum density vector. p represents thermodynamic pressure; $\mathbf{I}=\delta_{ij}\mathbf{e}_i\otimes\mathbf{e}_j$ defines unit tensor, and δ_{ij} is Kronecker's delta. Additionally, total diffusive momentum flux is defined as $\mathbf{t}^t=\mathbf{t}^{lam}+\mathbf{t}^{tur}$ and takes into account two components of viscous stress flux, namely, laminar and turbulent. $\rho\mathbf{S}_\mathbf{v}$ is momentum sources. The total specific energy $e=u+\frac{1}{2}\mathbf{v}^2$ includes specific internal energy u and specific kinetic energy $\frac{1}{2}\mathbf{v}^2$. $\mathbf{q}^t$ represents the total diffusive heat flux, and S_e are the energy sources. Furthermore, in the evolution part of the kinetic energy of turbulence k and dissipation of the kinetic energy of turbulence ε, occur diffusive fluxes of k and diffusive flux of ε, i.e. $\mathbf{J}_k$, $\mathbf{J}_\varepsilon$, respectively. The last but not least, in turbulence equations, sources, namely the source of the kinetic energy of turbulence S_k, together with the source of the dissipation of the kinetic energy of turbulence S_ε are the consequences in the flow which depend on many factors including cross effects with a phase transition. The additional balance equations for k, ε, x, and α are related to the evolution of turbulence in the condensing flow or the condensation evolution under turbulent flow conditions. Both are fully non-equilibrium phenomena that should be combined by the sources, S, and thermodynamical forces, which constitute the fluxes, $\mathbf{J}$. Transport of non-equilibrium properties between the phase and turbulent microstructure can be made directly on the microstructure level, without exploring the total momentum equation. It may be done by introducing the crossing effects in phase and turbulence fluxes:

- firstly by turbulent kinetic energy k [m^2/s^2]: $\mathbf{J}_k=D_{kk}\operatorname{grad}k+(D_{kxo}+D_{kxr})\operatorname{grad}x$;

- Secondly by dryness fraction x [-]:

$$\mathbf{J}_x = (D_{kxo}+D_{kxr})\ \text{grad}\ k + (D_{xxo}+D_{xxr})\ \text{grad}\ x$$

- Furthermore by turbulent energy dissipation rate ε [m^2/s^3]: $\mathbf{J}_\varepsilon = D_{\varepsilon\varepsilon}\ \text{grad}\ \varepsilon + (D_{\varepsilon\alpha o}+D_{\varepsilon\alpha r})\ \text{grad}\ \alpha$
- Finally by interphase surface density α [m^2/m^3]: $\mathbf{J}_\alpha = D_{\alpha\varepsilon}\ \text{grad}\ \varepsilon + (D_{\alpha\alpha o}+D_{\alpha\alpha r})\ \text{grad}\ \alpha$

where we introduces diffusion coefficients D, which are related with homogeneous diffusion known as the Ostwald mode (subscript o) and heterogeneous condensation mode (subscript r). It should be added, that the following assumptions are made in this model:

- the velocity slip between the droplets and gaseous-phase is negligible,
- the interactions between droplets are neglected.

The above set of nine equations is to be integrated within every finite volume. The process of growth of individual droplets is governed by mass, momentum, and energy transport mechanisms between gas and liquid phases.

The system of CSD equations may be written in a conservative form as follows [19]:

$$\frac{\partial}{\partial t}\begin{Bmatrix}\rho\\ \rho\mathbf{v}\\ \rho e\\ \rho\mathbf{e}^{pl}\\ \rho\boldsymbol{\alpha}\\ \rho r\end{Bmatrix} + \text{div}\begin{Bmatrix}\rho\mathbf{v}\\ (\rho\mathbf{v}\otimes\mathbf{v})\\ \rho e\mathbf{v}\\ \rho\mathbf{e}^{pl}\otimes\mathbf{v}\\ \rho\boldsymbol{\alpha}\otimes\mathbf{v}\\ \rho r\mathbf{v}\end{Bmatrix} = \text{div}\begin{Bmatrix}0\\ \boldsymbol{\sigma}\\ \boldsymbol{\sigma}\mathbf{v}+\mathbf{q}^{\text{c}}\\ 0\\ 0\\ \mathbf{J}_r\end{Bmatrix} + \begin{Bmatrix}0\\ \rho\mathbf{b}\\ \rho S_e\\ \rho\mathbf{S}_{pl}\\ \rho\mathbf{S}_{\boldsymbol{\alpha}}\\ \rho S_r\end{Bmatrix} \qquad (3)$$

where additionally, in comparison to (2), there appear such quantities as: $\boldsymbol{\sigma}$ - tensor of stresses in the solid; $\mathbf{e}^{pl}$- tensor of plastic strain; $\boldsymbol{\alpha}$ - kinematic hardening; r – isotropic hardening; $\mathbf{J}_r$ - diffusive flux of r ; $\mathbf{S}_{pl}$, $\mathbf{S}_{\boldsymbol{\alpha}}$, and S_r sources of plasticity, kinematic and isotropic hardening typical for the Chaboche model. The Chaboche model is appropriate because it is clearly defined and supported by many examples of calibration constants. It is fully temperature-dependent, so it can describe the thermal and mechanical stresses and visco-plastic deformations. The Chaboche model consists of well-known elements of continuum mechanics. On the other hand, on the influence occurring in the steam storage itself on the area of water vapor-water separation in the 0D approach, we put the following equations of the balance [14]:

$$\frac{\mathrm{d}\rho_{phase}}{\mathrm{d}t} V_{phase} = \sum_{i=1}^{n_{in}} \dot{m}_{in,phase,i} + \sum_{j=1}^{n_{out}} \dot{m}_{out,phase,j} + \dot{m}_{phase\_ch} + \frac{\mathrm{d}V_{phase}}{\mathrm{d}t} \rho_{phase} \quad (4)$$

$$\frac{d(mh)_{phase}}{dt} = \sum_{i=1}^{n_{in}} \dot{m}_{in,phase,i}\, h_{in,i} + \sum_{j=1}^{n_{out}} \dot{m}_{out,phase,j}\, h_{out,j} + \dot{m}_{phase\_ch} h' + \dot{m}_{phase\_ch} h'' + \frac{d(pV)_{phase}}{dt} + \dot{Q}_{wall,phase} + \dot{Q}_{phases} \quad (5)$$

where: ρ_{phase} is the density of liquid or vapor of water, V_{phase} represents the volume of liquid or vapor; $\dot{m}$ is mass flow rate; i is a number of inlets; j represents the number of outlets; and $\dot{m}_{phase\_ch}$ is mass flow rate obtain due to condensation or evaporation depending, which phase is balanced. The rate of energy obtained due to phase change is specified by $\dot{Q}_{phases}$, however, the rate of energy transferred through the wall of steam storage is taken into account as $\dot{Q}_{wall,phase}$. Three types of enthalpy are included in the balance of energy water/steam mainly: saturated water h'; dry saturated steam h'' and wet steam h. It is worth noting the pV component, which describes the amount of mechanical work accumulated during charging or discharge.

3 A concept of the thermodynamic cycle with steam storage for 0D modeling

The primary objective of introducing a steam storage facility is to increase the flexibility of steam units while maintaining operational safety and low emission levels. The special aim is to increase the power rate and extend the operating spectrum relative to the nominal load. In terms of thermodynamics, the aim of steam storage is to improve the primary control range by about 3% of the power output fluctuations and high ramp rates, both at power peaks and power downs, which at power peaks is twice the changeover rate. On the other hand, as it comes to operating range, it is possible to increase the power of the block after the integration of the steam storage by more than 3% or to reduce the power of the block when the minimum power of the discharged steam storage tank is reached by a further half percent. However, the exact values depend on the specificity of the block and the size of the storage tank to be integrated into the cycle.

To model the operation of the thermal cycle with a steam accumulator, a lignite-fired steam power plant block with a condensing turbine with a nominal power of 238 MW was analyzed. The block operates at a pressure of 13.17 MPa and a temperature of 540°C. Figure 2

shows items: B, the boiler; HP, IP, and LP, the high pressure, medium pressure, and low-pressure parts of the steam turbine, respectively; D, the deaerator; $HE_1 - HE_6$, the regenerative heat exchangers; P, the pump; G, the generator; and CON, the condenser. In the presented system, seven regenerative exchangers (D+$HE_1 - HE_6$) are used to heat the feedwater and the interstage heat in which the steam is heated to the temperature 540°C. Power plant parameters in the most important point of the cycle are presented in Table 1. Based on the warranty measurements, the efficiency of the system at variable load was calculated. The performed calculations were compared with the measured values. Parameters of the most significant devices are presented in Table 2.

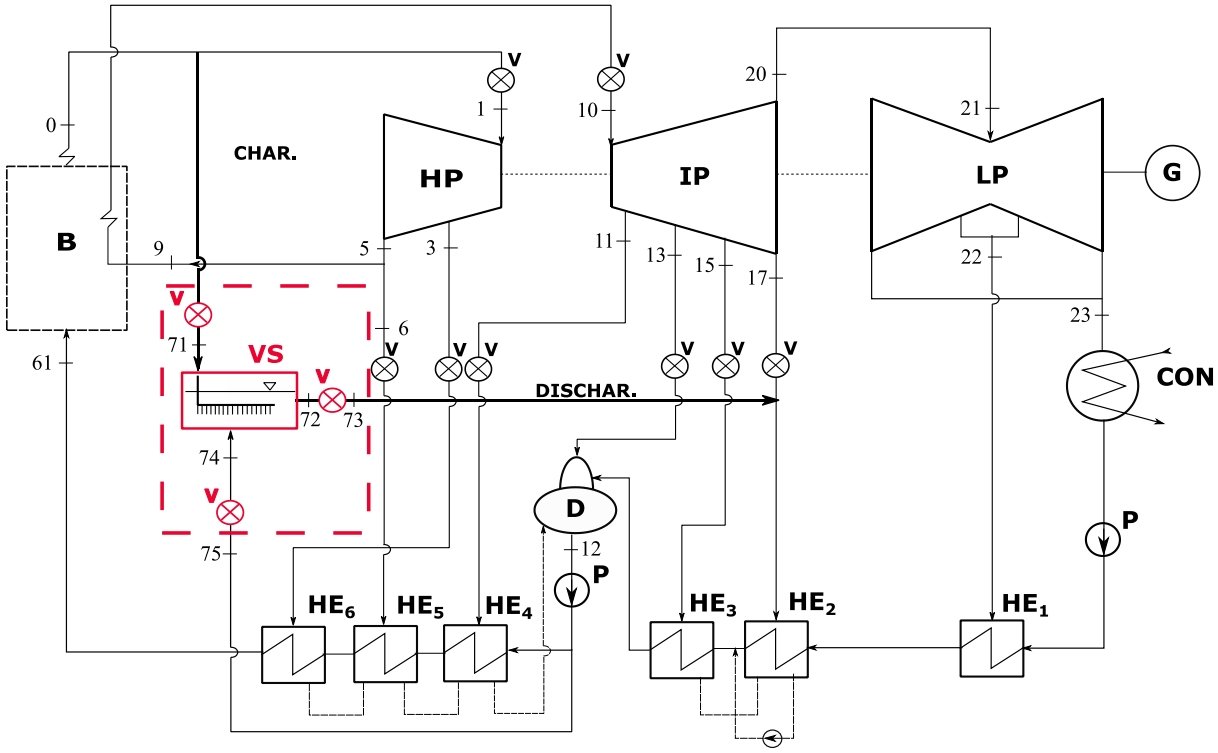

Fig. 2. General scheme of the steam block with the designation of basic devices cooperating with an innovaive steam store (VS) with charging (CHAR.) and discharging (DISCHAR.) pipeline.

Table 1. Steam parameters in the most important point of the thermodynamic cycle in nominal conditions.

Measurement points		Characteristic parameters of steam		
Number of the measurement point	Location of the measurement point	p [MPa]	t [°C]	$\dot{m}$[kg/s]
0	live steam	13.51	529.3	196.75
1	steam at the inlet to HP	13.32	529.3	195.64
3	steam to HE_6	3.91	352.3	7.56
5	steam at the outlet from HP	2.95	317.8	186.88
6	steam to HE_5	2.95	317.8	13.30
10	steam at the inlet to IP	2.51	541.7	172.98
11	steam to HE_4	1.43	462.0	11.54
13	steam to deareator	0.54	322.3	3.05
15	steam to HE_3	0.37	272.6	7.24
17	steam to HE_2	0.17	204.4	10.66
20	steam at the outlet from IP	0.15	174.4	140.07
21	steam at the inlet to LP	0.15	174.4	140.07
22	steam to HE_1	0.02	64.6	4.24
23	steam at the outlet from LP	0.01	38.6	135.97
12	deareator	0.53		4.37
61	feed water to the boiler	16.07	244.6	197.98
9	water to reheater			173.57

Where the steam storage is integrated into the heat cycle is shown in Fig. 2, including the various elements: B, the boiler; HP, IP, and LP, the high-pressure, medium-pressure, and low-pressure parts of a steam turbine, respectively; D, the deaerator; HE_1-HE_3, the low-pressure regenerative heat exchangers; HE_4-HE_6, the high-pressure regenerative exchangers; P, the pump; G, the electric generator; CON, the condenser; and V, the valves. The location of the steam storage (VS) with a suitable valve system on the live steam path provides a greater possibility of

regulating the amount of steam that goes to the high-pressure, medium-pressure, and steam used for regeneration in the high-pressure exchangers. Thus, this position of the steam store (VS) provides the possibility to use the live steam. This gives greater flexibility to the block and provides the ability to change power output faster than traditional systems both at full power and with a technical minimum. In addition, this integration ensures a smooth steam extraction from the boiler and adjustable turbine power output reduction. Figure 2 also shows the place of return of the medium stored (wet steam) in the steam storage to the low-pressure regeneration exchanger (HE_2), which allows increasing the water temperature in this heat exchanger.

Table 2. Efficiencies and losses are assumed in devices of the thermodynamic cycle.

Parameter	Symbol	Unit	Value
Boiler efficiency	η_B	-	0.9215
Generator efficiency	η_G	-	0.997
Mechanical efficiency	η_m	-	0.991
Pipelines efficiency (1 - heat losses of pipelines and medium)	η_{pip}	-	0.979
The internal efficiency of the HP turbine group of stages	η_{iHP}	-	0.859
The internal efficiency of the IP turbine group of stages	η_{iIP}	-	0.923
The internal efficiency of the LP turbine group of stages	η_{iLP}	-	0.737
Pressure loss in the reheater	ζ_{re}	%	4.7

Based on the measured pressure and temperature values (Table 1), the enthalpy of the working medium at characteristic points was determined:

$$h = f(p,t) \tag{6}$$

The values of the determined enthalpies and the mass flow rate were used to determine the power generated by the individual casings of the steam turbine:

$$N_{HP} = \dot{m}_1(h_1 - h_3) + (\dot{m}_1 - \dot{m}_3)(h_3 - h_5) \tag{7}$$

$$\begin{aligned} N_{IP} &= \dot{m}_{10}(h_{10} - h_{11}) + (\dot{m}_{10} - \dot{m}_{11})(h_{11} - h_{13}) \\ &+ (\dot{m}_{10} - \dot{m}_{11} - \dot{m}_{13})(h_{13} - h_{15}) \\ &+ (\dot{m}_{10} - \dot{m}_{11} - \dot{m}_{13} - \dot{m}_{15})(h_{15} - h_{17}) \end{aligned} \tag{8}$$

$$+(\dot{m}_{10} - \dot{m}_{11} - \dot{m}_{13} - \dot{m}_{15} - \dot{m}_{17})(h_{17} - h_{20})$$
$$N_{LP} = \dot{m}_{21}(h_{21} - h_{22}) + (\dot{m}_{21} - \dot{m}_{22})(h_{22} - h_{23}) \quad (9)$$

The heat flux supplied to the system in the boiler, and interstage heat was also determined:

$$\dot{Q}_d = \frac{\dot{m}_{21}(h_{21} - h_{22}) + (\dot{m}_{21} - \dot{m}_{22})(h_{22} - h_{23})}{\eta_B} \quad (10)$$

The gross efficiency of electricity production was determined based on the determined power values of individual turbine hulls and the heat supplied to the system:

$$\eta = \frac{N_t \eta_m \eta_G}{\dot{Q}_d} = \frac{(N_{HP} + N_{IP} + N_{LP})\eta_m \eta_G}{\dot{Q}_d} \quad (11)$$

where: N_t is the total power, N_{HP} is the power obtained from the high-pressure part of the turbine, N_{IP} is obtained from the medium-pressure part of the turbine, and N_{LP} is obtained from the low-pressure part of the turbine; the calculations were made with the assumptions (Table 2).

It should be mentioned that control methods are currently carried out, for example, with steam temperature control by water injection. Another method of regulation also applies to the boiler area and is related to the amount of fuel supplied to the burners and, therefore, the heat transfer rate on the waterwall furnace tubes. The introduction of an innovative steam storage tank will support the block by giving it an alternative method of primary control.

An additional profit is emission reduction of these units as the amount of burned fuel and emission efficiency of the whole unit is connected with the proper running of the unit. Therefore the introduced steam store will also have a direct impact on emission reduction of the power plant unit. Based on the steam store, it is possible to regulate the operation of the unit not only in dynamic conditions but also to optimize efficiency and reduce emissivity in transient states.

Table 3 presents the key parameters of the power plant, which is analyzed as a reference case. The referent efficiency $\eta_{re} = 0.3846$, and the gross electrical power of the power plant have been estimated as $N_{elGr} = 231.6$ MW by the numerical analysis. The calculations made for various load conditions of the block were compared with the results obtained by measurements (Table 3). The values obtained based on the calculation model slightly differ from the values determined by the measurement. This difference is less than 2.1% for power and less than 2.2% for efficiency. However, the results show that the calculation model was validated correctly. The

indicated differences (Table 3) are acceptable because the aim is to estimate the influence of the steam storage on the operation of any unit and not a detailed analysis of the primary circulation. On the other hand, detailed analyzes of classical cycles without steam stores were carried out in earlier works by the authors [16]. The difference presented in Table 3 results from the simplifications adopted in the calculation model, in which flow losses in steam pipelines and leakages in seals are omitted. The model also uses a simplification to determine the expansion line of the working medium in the low-pressure part of the turbine. Because of that, the parameters of the extraction steam supplying the HE_1 exchanger and the parameters at the outlet of the LP part may slightly differ from the actual values, which in turn affects the obtained results. The presented differences also result from the conditions adopted in the computational model, in which the determined thermodynamic parameters were determined for the stationary operation state.

Table 3. The calculations made for various load conditions compared with the results obtained by measurements.

Measurements		Calculations	
Electric power	Efficiency	Electric power	Efficiency
[MW]	[%]	[MW]	[%]
235.56	38.56	231.6	38.46
200.28	38.58	196.8	38.15
165.37	37.8	162.4	38.26
139.6	36.07	136.7	36.86
94.15	34.07	92.3	34.35

The next step was to check how the change in power and efficiency of the steam block is influenced by the cooperation of the system with the steam accumulator. The place where the steam storage (VS) is integrated into the heat cycle is shown in Fig. 2.

In the presented concept, the steam storage is supplied with live steam taken from the pipeline downstream of the boiler. It was assumed that 10% of the produced steam flows into the accumulator during loading. Steam intake after the boiler reduces the amount of the working

medium expanding in the high-pressure (HP), medium-pressure (IP), and low-pressure (LP) parts of the turbine, which causes a significant decrease in the power of the block.

According to this concept, the storage is unloaded to the extraction pipeline supplying the regenerative exchanger HE_2. This way, the mass flow rate in the low-pressure (LP) part of the turbine is increased, which contributes to a slight increase in the power of the block.

Assuming that the steam boiler workload remains unchanged at a given block load, the steam storage, depending on whether it is loaded or unloaded, may affect the power control of the block. By causing its increase or decrease that also affects the efficiency of the block. Based on the computational model, the power and efficiency of the steam unit cooperating with the steam accumulator were determined. Calculations were taken both for the state in which the tank is filled with steam and for the state in which the unloaded tank supplies to the heat exchanger HE_2 (Table 4).

Table 4. The calculations of the block both while loading steam storage and unloading steam storage made for various loads.

Operation of the block without steam storage		Operation of the block while loading steam storage		Operation of the block while unloading steam storage	
Electric power	Efficiency	Electric power	Efficiency	Electric power	Efficiency
MW	%	MW	%	MW	%
231.6	38.46	204.1	34.31	235.5	38.87
196.8	38.15	173.7	34.28	200.1	38.78
162.4	38.26	143.5	34.43	165.0	38.87
136.7	36.86	121	33.2	138.7	37.39
92.3	34.35	81.77	30.9	93.4	34.78

The values in Table 4 show that in the case of operation of the unit with a load close to the nominal load, loading the steam storage causes a decrease of the generated electric power by nearly 27.5 MW. As the power decreases, the efficiency of the block decreases by about 4.15%. Similar results were obtained in other work [14], where in the case of loading the tank at full load of the unit, a 5% decrease in efficiency was noted. Under the same load conditions of the block, discharging the accumulator increases the generated power by 3.9 MW, which results in an increase in the system efficiency by 0.41%. In this case, the results obtained by [14], which

indicates an increase in efficiency by 4.3%, differ significantly from the results presented here. The difference in the obtained results was undoubtedly influenced by various assumptions regarding the operating parameters of the steam store itself and the location of the discharge point of the stored medium in the cycle.

4 3D modeling of steam storage tank

The research method should combine theoretical and experimental issues in such a way as to obtain a calibration and verification of a steam storage facility cooperating with a steam block. Therefore, the test method must take into account:

- the zero-dimensional method (0D), in other words, mass, momentum, and energy balancing at the level of the steam storage, so as to implement this data to the whole block;
- the three-dimensional (3D) method, which allows knowing exactly the mechanisms governing the processes inside the steam store and their influence on the stresses in the tank walls.

In the process of calibrating the numerical model, it is important to have a measuring system that collects the response of the steam accumulator depending on the parameters and the amount of steam introduced into it. In the case of the benchmark experiment, the steam source will be an LW40 steam generator from Prometr with a 28 kW heating system. Connecting it to the steam storage tank provides the measurements necessary to determine the 0D and 3D characteristics necessary to verify the models and their constants. The steam generator includes an electric boiler, a water pump, and a condensate tank. The boiler capacity will be 50 L, and the nominal steam output is 40 kg/h (Fig. 3). Achievable thermal parameters for the generator are 180°C and 8 bar.

The generator is equipped with a centrifugal pump and a stainless-steel condensate tank with a capacity of 75 L. The steam generator has its own capacity control system and a protection system against excessive steam pressure increase in the boiler. Therefore, the steam generator is fully sufficient to take the necessary measurements and obtain both integral and spatial parameters in the time needed to obtain calibration characteristics. The experiment aims to capture first the integral parameters of the steam storage, i.e., at the inlet and outlet of the tank, on the basis of which a mathematical model described by integral equations can be calibrated. It should be mentioned that experimental results are available in the literature [24,25], but they are aimed at obtaining integral characteristics, i.e., at the 0D approach. In turn,

the concept of the experiment from this work is to indicate the parameters at different points of the steam storage to obtain variability in the 3D space, and thus the measuring system contains several sensors of temperature and pressure after height, width, and length of the tank. In addition, time displacements are measured to determine the thermal effects of a sudden inflow of steam into the steam storage. The geometry created is then used for numerical analysis of the CFD type.

At the same time, CFD flow analysis results will become boundary parameters for stress/strength analyses, where not only pressure changes acting on the tank walls but also process temperature changes will be important. With such diverse operating parameters, it would be appropriate to consider material fatigue and creep effects. For extremely loaded elements, the risk of plasticisation and the conditions of material strengthening in an isotropic and kinetic way should be investigated [26–28]. It is also worth adding that the 3D analysis of the stream flows in the innovative steam accumulator will be carried out considering the boundary conditions from the analysis of the cycle in the context of geometry (Fig. 3) optimization, taking into account pressure drops, mass, and heat transfer. The stress/strength analysis of the steam storage tank will harness the variable operating parameters to determine minimum wall thicknesses and dynamic transient forces.

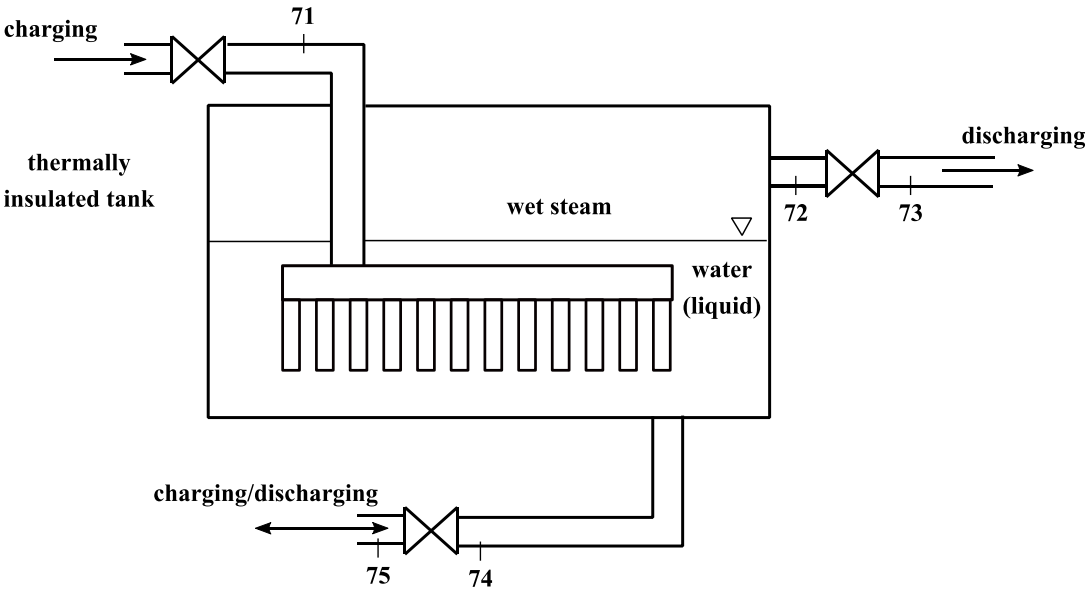

Fig. 3. A scheme of an innovative steam storage facility, which will be measured to perform a benchmarking experiment. The main parameters measured in time will be pressure, temperature, mass flow rates, the water level in the tank and displacement.

However, at this stage of the work, it was decided to model simplified steam storage (Fig. 4) to demonstrate the ability of 0D codes to work with 3D codes. Steam storage was modeled as a cuboid of dimensions 4.75 × 3 × 4 m with two fluids (water and steam) in it. The volume of the storage, 57 m^3, corresponds to the needs of the actual steam cycle. The tank is filled up to 70% of height with water where four steam inlet pipes were placed (Fig. 4right side). Steam domain and inlet pipes are shown in Fig. 4 (left side).

A large part of the research, considering steam condensation in water, focuses on sparging or steam jets [29–31]. Both mentioned processes consider the relatively high magnitude of the velocity of the steam or significantly higher pressure than in the described case.

A comparable phenomenon, but with only 2D calculations, was described [32] according to pool systems of Boiling Water Reactors. It differs from applications with steam jets because it presents low Reynolds number simulations. The authors focused on condensation mass flux near blowdown pipe.

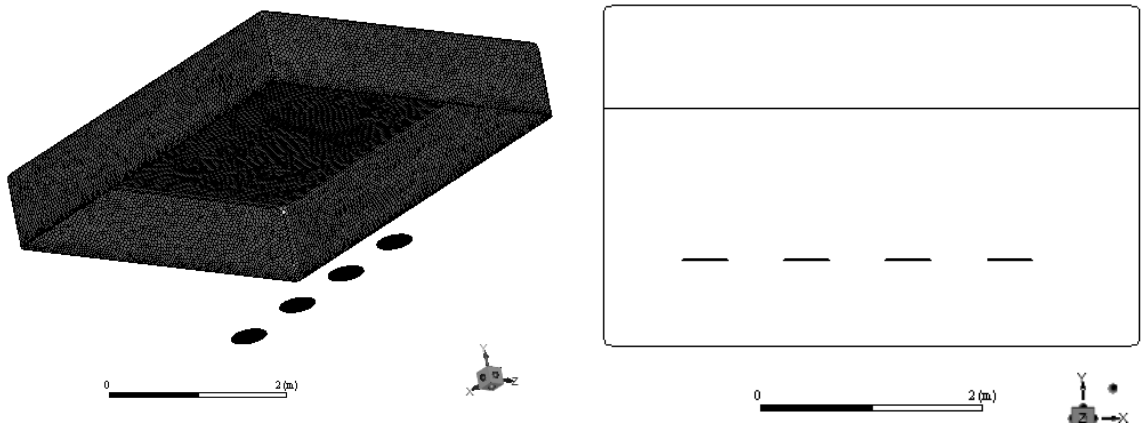

Fig. 4. On the left, an overview of the chosen mesh areas. On the right, the intersection of the model shoving the inlets.

The geometry in Fig. 4 was discretized with polyhedral mesh that consists of 1306258 elements. Water and steam zones were separated. According to state of the art, the mesh was refined in crucial areas. On the presented mesh, simulations using PISO pressure-velocity coupling scheme were performed. First-order upwind discretization was used for: density,

momentum, turbulent kinetic energy, turbulent dissipation rate. The energy was discretized with second-order upwind and pressure with PRESTO! Scheme.

Steam was injected into the storage at 5.6 bar and 530°C. The first 1.2 s of injecting of the steam into the accumulator were simulated. Fig. 5 presents the distribution of density in the storage tank at time 0.0 s - phases in balance. The tank is filled with water up to 2.1 m in height.

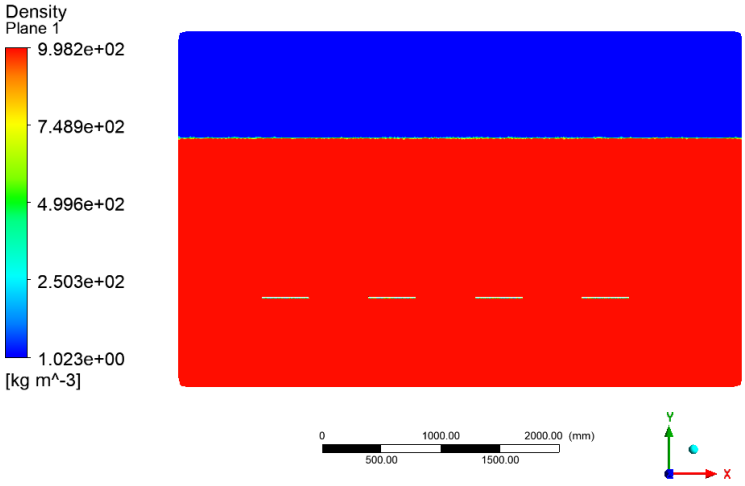

Fig. 5. Field of density in time 0.0 s.

Table 5 presents a comparison of the density and temperature over time. Mixing of both phases is visible also the process of saturation is noticeable. The temperature in the dominant volume of the tank is close to the saturation temperature for inlet steam pressure.

Fig. 6 (field of density at time 1.2 s), joined with Fig. *7* (distribution of volume fraction), presents the phenomenon from the side of phase change. Both of them show distributions of y-axis intersection left: on level of inlet pipes, right: on height 2.1 m. The calculations take into account the full two-phase model, including condensation and evaporation, the model of the tank was mapped at full scale in order to fully reflect the phenomena occurring inside. The calculations consider the full two-phase model, including condensation and evaporation, the model of the tank was mapped at full scale in order to fully reflect the phenomena occurring inside. The size of the geometry forces some simplifications in terms of mesh accuracy, which, compared to the significant steam flow velocities, results in the occurrence of a high CFL values. To maintain the stability of the calculations, the time steps must be kept on the order of 0.00001 of a second. The simulation showed that over a period of 1 second by changing the pressure inside the tank and due to cooling of the inlet steam, 43 kg of steam condensed in the tank.

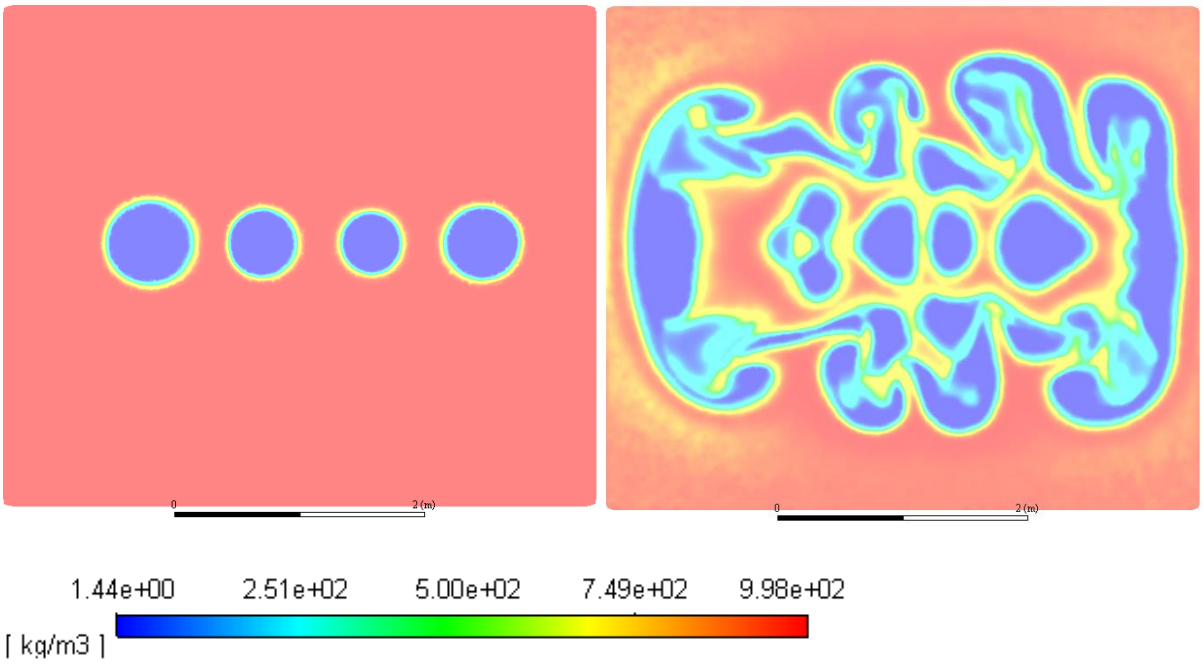

Fig. 6. Field of density at time 1.2 s, y-axis intersection left: on level of inlet pipes, right: on height 2.1 m. Maximum density (red) 998 $\left[\frac{kg}{m^3}\right]$*, minimum (blue) 144* $\left[\frac{kg}{m^3}\right]$

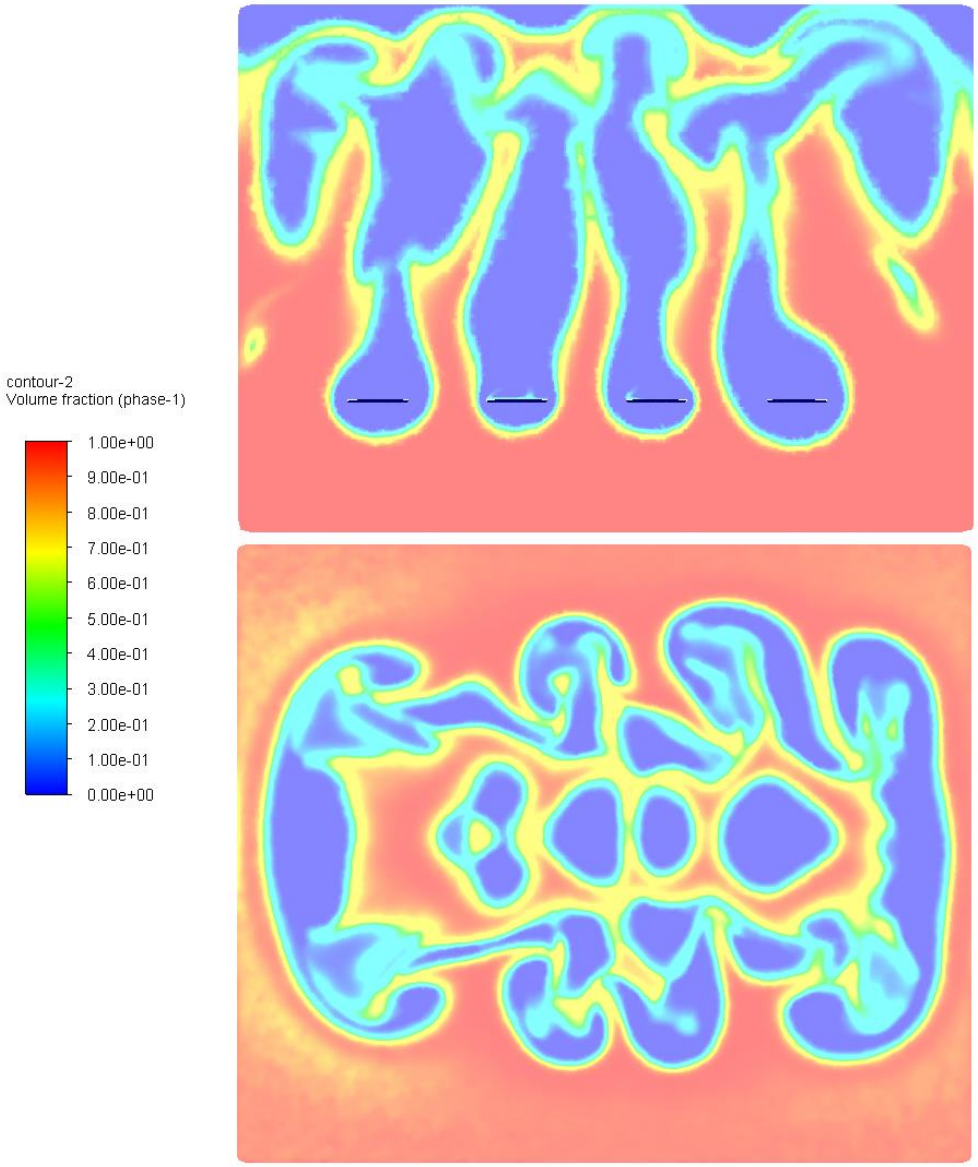

Fig. 7. Phase transition field. Volume fraction field. Time: 1.2 s. Up: z-axis intersection, Down: x-axis intersection at 2.1 m height of the tank.

Owing to the fact, that in 0D model most accurately is computed the average (theoretical) velocity, it is easier to formulate the ideal mass flow rate $\dot{m}_t$, than real mass flow rate $\dot{m}$. Hence, the real mass flow rate, which according to the velocity profile is always lower, may be described with the empirical flow capacity coefficient μ:

$$\dot{m} = \mu\, \dot{m}_t \tag{12}$$

In the 0D modeling practice, mass flow rate coefficient determination bases on computing the ideal mass flow rate $\dot{m}_t$ and measuring the real mass flow rate $\dot{m}$:

$$\mu_{0D} = \frac{\dot{m}_{exp}}{\dot{m}_{t,0D}} \tag{13}$$

Experiments are possible to perform in small channels, measuring techniques conducted *in situ*, however in our case is considered steam storage tank for power plant.
In the case of 3D modeling – the real mass flux $\dot{m}$ is accurately computed, and interpretational difficulties arise with the theoretical $\dot{m}_t$. When both mass flow rates are computed with use of the same numerical tables of state, for the change of state, the mass flow rate coefficient may be determined for each devices as:

$$\mu_{CFD} = \frac{\dot{m}_{CFD}}{\dot{m}_{t,CFD}} \tag{13}$$

The μ_{CFD} coefficient is slightly smaller than μ_{0D}, nonetheless, for design purposes it may be assumed that $\mu_{0D} = \mu_{CFD}$. From results given in 0D approach and 3D approach it concludes that the coefficient μ_{CFD} for the CFD calculations according to Fig.8, is $\mu_{CFD} = 0.905$ for assumed dimensions.

It requires noting, that the mass flow rate computed in CFD is the basic integral parameter of the 3D flow, which is controlled during the numerical process – it is possible to be read in any section *A* (not necessarily planar) of a tank flow domain, oriented with a normal vector **n** as:

$$\dot{m}_{CFD} = \iint_A \rho\, v_n\, dA = \iint_A \rho\, \mathbf{v} \cdot \mathbf{n}\, dA \tag{14}$$

where the normal to surface velocity component magnitude v_n occurs, not the entire magnitude of the vector. Transition to the 0D model is as follows [17]:

$$\dot{m}_{0D} = \iint_A dA\, \frac{\iint_A \rho\, dA}{\iint_A dA}\, \frac{\iint_A \rho\, v_n\, dA}{\iint_A \rho\, dA} = A\tilde{\rho} c_n = A\rho\mu_{0D} c_t = \mu_{0D}\dot{m}_{t,0D} \tag{15}$$

The flow capacity coefficient depends on both the fact, that the average velocity c_n determines the constant velocity profile within the section, and that $c = \varphi c_t$ and the direction of the averaged vector **c** is unknown, that enforces assuming $c_n = \mathbf{c} \cdot \mathbf{n} \cong c$. Velocity profiles obtained at the steam inlets to the tank, together with an approximation to one of the inlets are presented in Figure 8.

Determining the condensation velocity as well as the vapor distribution in the tank (to assist in the design of inlet size and placement) would not be possible without 3D analysis.

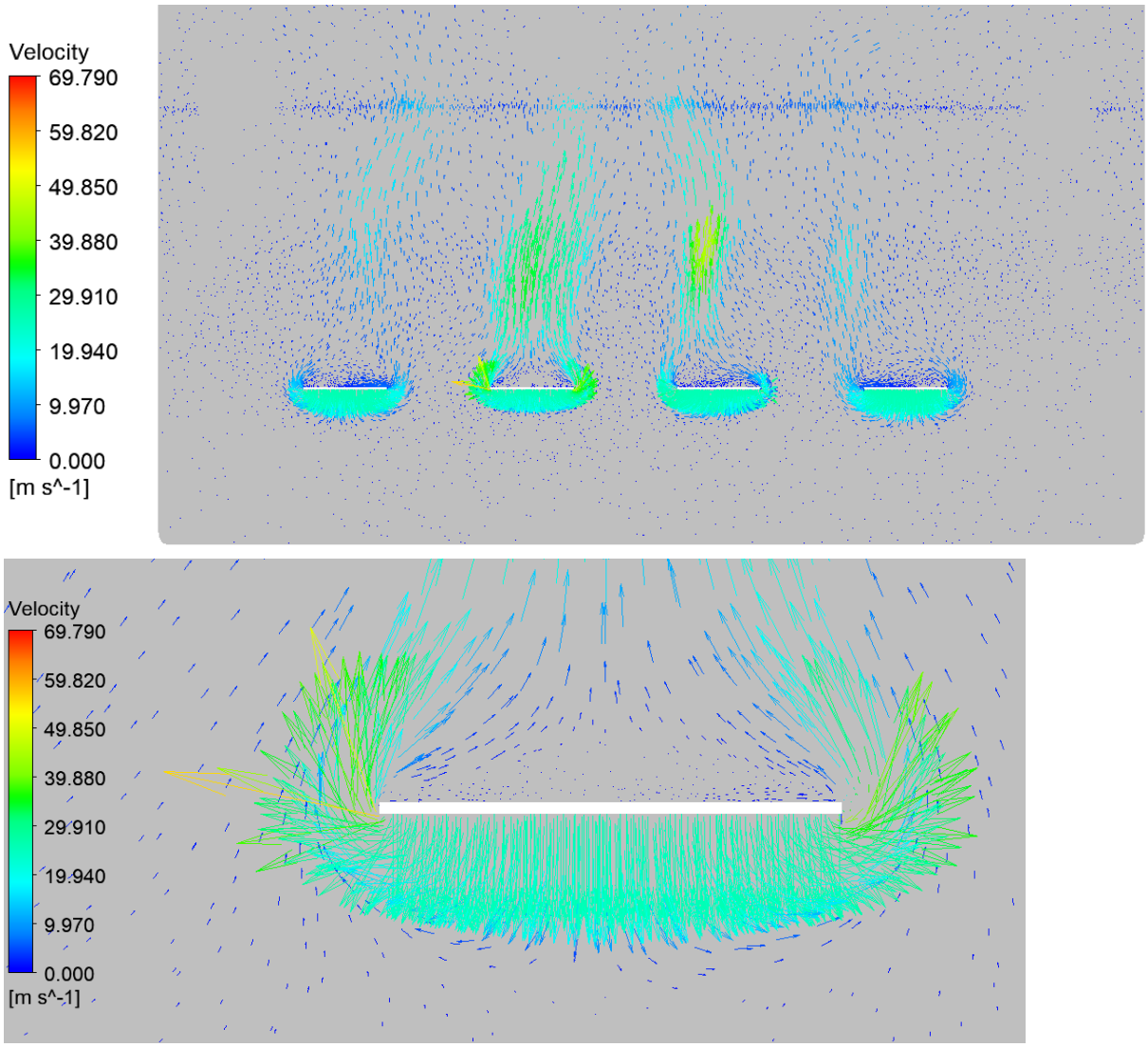

Fig. 8. Velocity profiles obtained at the steam inlets to the tank, together with an approximation to one of the inlets.

Table 5. Z-axis intersection of the tank, field of density and temperature in time. Density minimum 9.15e-01 $\left[\frac{kg}{m^3}\right]$*, maximum 9.98e+02*$\left[\frac{kg}{m^3}\right]$*. Temperature minimum 404[K], maximum 802[K]*

Time [s]	Density	Temperature
		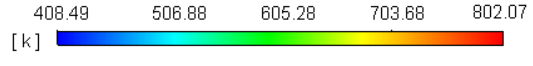
0.3	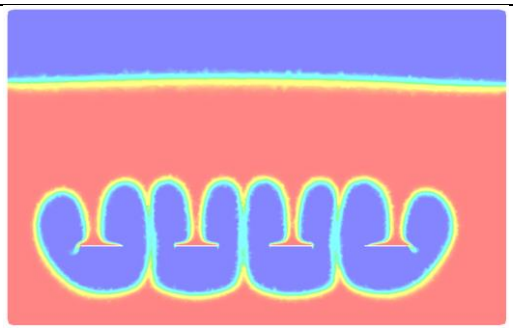	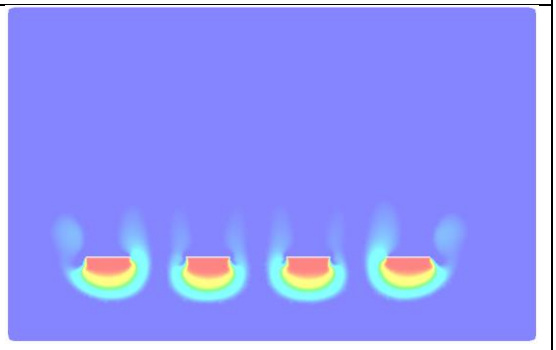
0.7		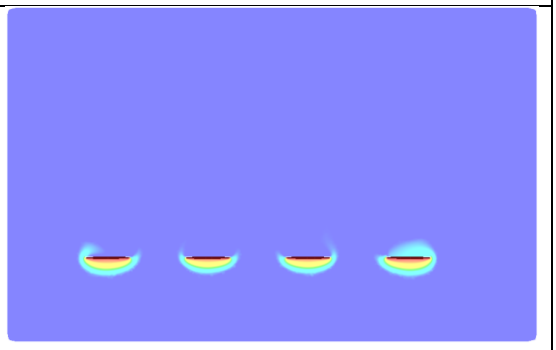
1.2	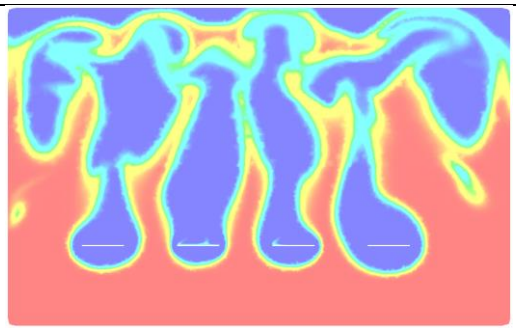	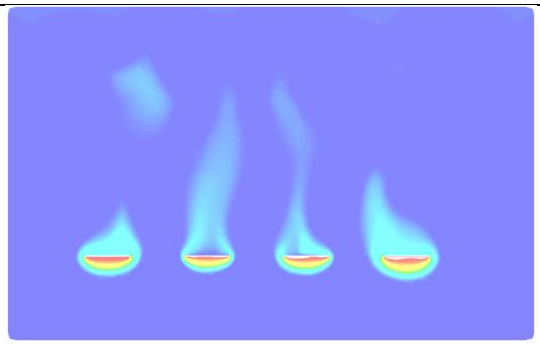

5 Conclusions and perspectives

The scientific value of implementing the presented concept and carrying out the research is related to the development of numerical methods and their coupling with each other. In the

future, an important scientific value will be the calibration of the steam store on one in-house experiment. At this point, it is worth adding that the phenomenon accompanying the calculations based on 3D models is a renaissance of significance and almost complete restoration of the equivalent significance of calculation codes based on 0D models. It should be remembered that 0D codes covering the entire turbine and thermodynamic cycle thus serve 3D codes (for both liquid and solid) as a "giver" of boundary conditions and averaged (in the 0D sense) load data. Furthermore, the results of the 3D calculation, after appropriate averages, are compared to the results of the 0D codes, especially at the solution design stage when no measurement data is yet available. The scientific value is also enhanced by the fact that the calibration will take place in a dedicated experiment considering the dynamic effects.

The novelty of the proposed concept consists of the use of advanced numerical tools and the theory of thermal-FSI to non-stationary model phenomena. The fact that steam storage fits perfectly into the primary control of the unit and can be installed close to the boiler is also innovative. However, alternatives are available, such as liquefied-air storages [33] or hydrogen-producing storage [34]. In the era of intensive development of wind and photovoltaic power plants, a very important aspect is the dynamics of load changes in power plants (Central Power Generating Units) [35]. Steam storage tanks are installations aimed at improving the flexibility of electricity generation in power units. However, the steam storage tanks themselves operate at high parameters. Therefore, it is important to propose solutions that not only have high efficiency of the charge/discharge cycle, the so-called round-trip-efficiency but above all can be dynamically charged (charged/discharged). This requires a detailed analysis of the thick-walled components of such plants, which will be introduced in the next level of work. Their structural optimization and then operational optimization, in the sense of determining the optimum characteristics of the change in operating conditions as a function of temperature and pressure, will emerge at the last stage of work. It has also been repeatedly emphasized that the approach to the problem is innovative, which uses many computational tools to well reproduce the phenomena occurring in devices at the boundary between liquid and solid, then determine the size of the necessary foundations cooperating with the ground and properly introduce the characteristics of a completely new device into the block simulator.

An additional innovation is the fact that steam storage can be used both as a source of thermal energy flow and a source of mechanical power because the steam still retains its high-pressure gaseous form. With a proper introduction to the steam turbine, it will allow generating

electric energy, or in the case of units equipped with regenerative exchanger system, it will be used to raise water temperature. Therefore, the multi-tasking of this storage is important. In addition, it can be said that it is innovative to combine simple construction with high exergy storage. The steam storage tank is a kind of indirect solution between heat accumulator and electricity or fuel storage. Its construction is simple, which significantly reduces costs in comparison to SOEC solutions or electric batteries, without having to concern about electrolytes or excessive sensitivity to thermal stress. If we compare steam storage to a heat accumulator, the energy in it is significantly more exergic, which means that there is much more power generation and almost instantaneous system response.

Acknowledgments

Financial support of these studies from Gdańsk University of Technology by the DEC-50/2020/IDUB/I.3.3 grant under the ARGENTUM TRIGGERING RESEARCH GRANTS - EIRU program is gratefully acknowledged.

References

[1] Koytsoumpa, E. I., Bergins, C., Buddenberg, T., Wu, S., Sigurbjörnsson, Ó., Tran, K. C., and Kakaras, E., 2016, "The Challenge of Energy Storage in Europe: Focus on Power to Fuel," J. Energy Resour. Technol., **138**(4), pp. 1–10.

[2] Saadat, M., and Li, P. Y., 2012, "Modeling and Control of a Novel Compressed Air Energy Storage System for Offshore Wind Turbine," *2012 American Control Conference (ACC)*, IEEE, pp. 3032–3037.

[3] Chedid, R., Salameh, S., Karaki, S., Yehia, M., and Al-Ali, R., 1999, "Optimization of Electrical Distribution Networks Fed by Conventional and Renewable Energy Sources," Int. J. Energy Res., **23**, pp. 751–763.

[4] Khaitan, S. ., and Raju, M., 2011, "Dynamic Simulation of Air Storage-Based Gas Turbine Plants," Int. J. Energy Res., **37**, pp. 558–569.

[5] Mazloum, Y., Sayah, H., and Nemer, M., 2016, "Static and Dynamic Modeling Comparison of an Adiabatic Compressed Air Energy Storage System," J. Energy Resour. Technol., **138**(6), p. 062001.

[6] Upendra Roy, B. P., and Rengarajan, N., 2017, "Feasibility Study of an Energy Storage System for Distributed Generation System in Islanding Mode," J. Energy Resour. Technol., **139**(1), p. 011901.

[7] Mollenhauer, E., Christidis, A., and Tsatsaronis, G., 2018, "Increasing the Flexibility of Combined Heat and Power Plants With Heat Pumps and Thermal Energy Storage," J. Energy Resour. Technol., **140**(2), p. 020907.

[8] Yokoyama, R., and Ito, K., 1996, "A Revised Decomposition Method for MILP Problems and ITs Application to Operational Planning of Thermal Storage Systems," J. Energy Resour. Technol., **118**, pp. 277–284.

[9] Koohi-Fayegh, S., and Rosen, M. A., 2020, "A Review of Energy Storage Types, Applications and Recent Developments," J. Energy Storage, **27**(November 2019), p. 101047.

[10] Vadasz, P., and Weiner, D., 1987, "An Evaluation Method for Peak/off-Peak Price Functions in Energy Storage Technologies," J. Energy Resour. Technol. Trans. ASME, **109**, pp. 21–25.

[11] Chen, S., Zhu, T., and Zhang, H., 2019, "Study on Optimization of Pressure Ratio Distribution in Multistage Compressed Air Energy Storage System," J. Energy Resour. Technol., **141**(6), p. 061901.

[12] Kushnir, R., Ullmann, A., and Dayan, A., 2012, "Thermodynamic Models for the Temperature and Pressure Variations Within Adiabatic Caverns of Compressed Air Energy Storage Plants," J. Energy Resour. Technol., **134**(2), p. 021901.

[13] Pinelli, M., and Piva, S., 2003, "Solid/Liquid Phase Change in Presence of Natural Convection: A Thermal Energy Storage Case Study," J. Energy Resour. Technol., **125**(3), pp. 190–198.

[14] Richter, M., Oeljeklaus, G., and Görner, K., 2019, "Improving the Load Flexibility of Coal-Fired Power Plants by the Integration of a Thermal Energy Storage," Appl. Energy, **236**, pp. 607–621.

[15] Badur, J., Ziółkowski, P., Zakrzewski, W., Sławiński, D., Kornet, S., Kowalczyk, T., Hernet, J., Piotrowski, R., Felincjancik, J., and Ziółkowski, P. J., 2014, "An Advanced Thermal-FSI Approach to Flow Heating/Cooling," J. Phys. Conf. Ser., **530**(1), p. 012039.

[16] Ziółkowski, P., Kowalczyk, T., Kornet, S., and Badur, J., 2017, "On Low-Grade Waste Heat Utilization from a Supercritical Steam Power Plant Using an ORC-Bottoming Cycle Coupled with Two Sources of Heat," Energy Convers. Manag., **146**, pp. 158–173.

[17] Ziółkowski, P., and Badur, J., 2018, "A Theoretical, Numerical and Experimental Verification of the Reynolds Thermal Transpiration Law," Int. J. Numer. Methods Heat Fluid Flow, **28**(1), pp. 64–80.

[18] Ziółkowski, P., 2019, "Porous Structures in Aspects of Transpirating Cooling of Oxycombustion Chamber Walls," *AIP Conference Proceedings*, American Institute of Physics Inc., p. 020065.

[19] Badur, J., Kornet, S., Sławiński, D., and Ziółkowski, P., 2016, "Analysis of Unsteady Flow Forces Acting on the Thermowell in a Steam Turbine Control Stage," J. Phys. Conf. Ser., **760**(1), p. 012001.

[20] Dominiczak, K., Drosińska-Komor, M., Rządkowski, R., and Głuch, J., 2020, "Optimisation of Turbine Shaft Heating Process under Steam Turbine Run-up Conditions," Arch. Thermodyn., **41**(4), pp. 255–268.

[21] Banaszkiewicz, M., 2015, "Multilevel Approach to Lifetime Assessment of Steam Turbines," Int. J. Fatigue, **73**, pp. 39–47.

[22] Ziółkowski, P., and Badur, J., 2018, "On Navier Slip and Reynolds Transpiration Numbers," Arch. Mech, **70**, pp. 269–300.

[23] Kornet, S., and Badur, J., 2017, "Numerical Analysis of the Oscillation Frequency of the Shock Wave and the Evaporation Level on the Mach Disc in the IMP PAN Nozzle," Prog. Comput. Fluid Dyn., **17**(6), pp. 352–360.

[24] Stevanovic, V. D., Petrovic, M. M., Milivojevic, S., and Maslovaric, B., 2015, "Prediction and Control of Steam Accumulation," Heat Transf. Eng., **36**(5), pp. 498–510.

[25] Stevanovic, V. D., Maslovaric, B., and Prica, S., 2012, "Dynamics of Steam Accumulation," Appl. Therm. Eng., **37**, pp. 73–79.

[26] Ziółkowski, P. J., Ochrymiuk, T., and Eremeyev, V. A., 2019, "Adaptation of the Arbitrary Lagrange–Euler Approach to Fluid–Solid Interaction on an Example of High Velocity Flow over Thin Platelet," Contin. Mech. Thermodyn.

[27] Badur, J., Ziolkowski, P., Kornet, S., Stajnke, M., Bryk, M., Banas, K., and Ziolkowski, P., 2017, "The Effort of the Steam Turbine Caused by a Flood Wave Load," *AIP Conference Proceedings*, American Institute of Physics Inc., p. 020001.

[28] Badur, J., Bryk, M., Ziolkowski, P., Slawinski, D., Ziolkowski, P., Kornet, S., and Stajnke, M., 2017, "On a Comparison of Huber-Mises-Hencky with Burzynski-Pecherski Equivalent Stresses for Glass Body during Nonstationary Thermal Load," *AIP Conference Proceedings*, American Institute of Physics Inc., p. 020002.

[29] Kwidzinski, R., 2021, "Condensation Heat and Mass Transfer in Steam–Water Injectors," Int. J. Heat Mass Transf., **164**, p. 120582.

[30] Qu, X. H., Sui, H., and Tian, M. C., 2016, "CFD Simulation of Steam-Air Jet Condensation," Nucl. Eng. Des., **297**, pp. 44–53.

[31] Dahikar, S. K., Sathe, M. J., and Joshi, J. B., 2010, "Investigation of Flow and Temperature Patterns in Direct Contact Condensation Using PIV, PLIF and CFD," Chem. Eng. Sci., **65**(16), pp. 4606–4620.

[32] Patel, G., Tanskanen, V., and Kyrki-Rajamäki, R., 2014, "Numerical Modelling of Low-Reynolds Number Direct Contact Condensation in a Suppression Pool Test Facility," Ann. Nucl. Energy, **71**, pp. 376–387.

[33] "Https://Highviewpower.Com/Technology/" [Online]. Available: https://highviewpower.com/technology/.

[34] Kowalczyk, T., Badur, J., and Bryk, M., 2019, "Energy and Exergy Analysis of Hydrogen Production Combined with Electric Energy Generation in a Nuclear Cogeneration Cycle," Energy Convers. Manag., **198**, p. 111805.

[35] Hyrzyński, R., Ziółkowski, P., Gotzman, S., Kraszewski, B., Ochrymiuk, T., Badur, J., 2021, Comprehensive thermodynamic analysis of the CAES system coupled with the underground thermal energy storage taking into account global, central and local level of energy conversion. Renewable Energy, **169**, pp. 379–403.